Biochemistry

 Volume 42, Number 44 November 11, 2003

Current Topics

Structure and Function of Malic Enzymes, A New Class of Oxidative Decarboxylases†

Gu-Gang Chang*,‡ and Liang Tong§

Faculty of Life Sciences, Institute of Biochemistry, Proteome Research Center, National Yang-Ming University, Taipei 112, Taiwan, and Department of Biological Sciences, Columbia University, New York, New York 10027

Received July 16, 2003; Revised Manuscript Received September 24, 2003

ABSTRACT: Malic enzyme is a tetrameric protein with double dimer structure in which the dimer interface is more intimately contacted than the tetramer interface. Each monomeric unit of the enzyme is composed of four structural domains, which show a different folding topology from those of the other oxidative decarboxylases. The active center is located at the interface between domains B and C. For human mitochondrial malic enzyme, there is an exo nucleotide-binding site for the inhibitor ATP and an allosteric site for the activator fumarate, located at the tetramer and dimer interfaces, respectively. Crystal structures of the enzyme in various complexed forms indicate that the enzyme may exist in equilibrium among two open and two closed forms. Interconversion among these forms involves rigid-body movements of the four structural domains. Substrate binding at the active site shifts the open form to the closed form that represents an active site closure. Fumarate binding at the allosteric site induces the interconversion between forms I and II, which is mediated by the movements of domains A and D. Structures of malic enzyme from different sources are compared with an emphasis on the differences and their implications to structure−function relationships. The binding modes of the substrate, product, cofactors, and transition-state analogue at the active site, as well as ATP and fumarate at the exo site and allosteric site, respectively, provide a clear account for the catalytic mechanism, nucleotide specificities, allosteric regulation, and functional roles of the quaternary structure. The proposed catalytic mechanism involves tyrosine-112 and lysine-183 as the general acid and base, respectively. In addition, a divalent metal ion (Mn^{2+} or Mg^{2+}) is essential in helping the catalysis. Binding of the metal ion also plays an important role in stabilizing the quaternary structural integrity of the enzyme.

In a reflections article (*1*), Kornberg vividly described the way leading to the discovery and characterization of pigeon liver malic enzyme (ME)[1] (*2*). Later, this enzyme was found to be widely distributed in nature, in bacteria, plants, and animals. In mammals, malic enzymes have three identifiable isoforms: cytosolic $NADP^+$-dependent (c-NADP-ME) (EC 1.1.1.40), mitochondrial $NADP^+$-dependent (m-NADP-ME)

† Supported by the National Science Council, ROC (Frontiers in Sciences Program, NSC 91-2321-B-010-002 and International Cooperative Program, NSC 92-2321-B-012-066 to G.-.G.C.) and the National Science Foundation, USA (MCB-99-74700 to L.T.).

* Corresponding author. E-mail: ggchang@ym.edu.tw and tong@como.bio.columbia.edu.

‡ National Yang-Ming University.

§ Columbia University.

[1] Abbreviations: ME, malic enzyme; c-NADP-ME, cytosolic $NADP^+$-dependent malic enzyme; m-NAD-ME, mitochondrial $NAD(P)^+$-dependent malic enzyme; m-NADP-ME, mitochondrial $NADP^+$-dependent malic enzyme.

10.1021/bi035251+ CCC: $25.00
Published on Web 10/14/2003

(EC 1.1.1.40), and mitochondrial NAD(P)$^+$-dependent malic enzymes (m-NAD-ME) (EC 1.1.1.38). m-NAD-ME can use either NAD$^+$ or NADP$^+$ as the cofactor but prefers NAD$^+$ under physiological conditions (*3*). Distinct from c-NADP-ME and m-NADP-ME, m-NAD-ME is an allosteric enzyme with fumarate as an activator and ATP as an inhibitor (*3*).

Malic enzyme catalyzes a reversible oxidative decarboxylation of L-malate to give carbon dioxide and pyruvate in the concomitant reduction of NAD(P)$^+$ to NAD(P)H. The enzyme thus has a systematic name of (*S*)-malate:NAD(P)$^+$ oxidoreductase (oxaloacetate-decarboxylating). The reaction also needs an essential divalent metal ion (Mn^{2+} or Mg^{2+}) for the catalysis.

$$\text{NAD(P)}^+ + \text{L-malate} \overset{\text{Me}^{2+}}{\rightleftharpoons} \text{CO}_2 + \text{pyruvate} + \text{NAD(P)H} + \text{H}^+$$

c-NADP-ME was grouped as a lipogenic enzyme because of its involvement in providing NADPH for the biosynthesis of long-chain fatty acids or steroids (*3*−*5*). In C4 plants, ME is involved in the anaplerotic replenish of the tricarboxylic acid-cycle intermediate (*6*, *7*). Human m-NAD-ME has received much attention because of its involvement in the energy metabolism in neuron or neoplasia tissues (*8*−*11*). Mitochondrial malic enzyme could associate with the pyruvate dehydrogenase complex in the inner mitochondrial membrane. This could localize m-NAD-ME in the vicinity of the inner mitochondrial membrane, making m-NAD-ME able to intercept exogenous malate from malate dehydrogenase as malate passing through the inner mitochondrial membrane (*10*). This may be the reason that glutamine instead of glucose is the major energy source of some tumor cells (*9*). Mitochondrial malic enzyme is thus a potential target in cancer chemotherapy. A structure-based rational drug design for ME could lead to potential anti-cancer drugs. In this perspective, solving the first crystal structure of ME in 1999 (*12*) had a special impact in this important field.

There are a total of 13 crystal structures of ME available in the Protein Data Bank (Table 1, Supporting Information). All of these ME have similar overall tertiary structure albeit with small local differences, which have important structural implications on the catalytic and regulatory mechanisms. This review summarizes the structural features and the functional implications of this new class of oxidative decarboxylases.

Structural Studies of Malic Enzymes. Crystals of pigeon c-NADP-ME were first reported more than 30 years ago (*13*). Since then, crystals of other malic enzymes have also been obtained, including rat c-NADP-ME (*14*), *Ascaris suum* m-NAD-ME (*15*), human m-NAD-ME (*16*), and new crystal forms of pigeon c-NADP-ME (*17*). The first crystal structure of any malic enzyme is that of human m-NAD-ME, in a binary complex with NAD$^+$ (Table 1, Supporting Information) (*12*, *18*). This is followed by the structures of this enzyme in a ternary complex with NAD$^+$ and Lu^{3+} (*19*), quaternary complexes with NAD$^+$, substrate analogue inhibitors, and divalent cations (*20*); as well as pentary complexes with NAD$^+$, NADH, or the inhibitor ATP, substrate malate or pyruvate, divalent cation, and the allosteric activator fumarate (*21*, *22*). In addition, the structures of pigeon c-NADP-ME in a quaternary complex with NADP$^+$, oxalate, and a divalent cation (*23*), as well as *A. suum* m-NAD-ME in a binary complex with NAD$^+$ or quaternary complex with NADH, tartronate, and Mg^{2+} (*24*, *25*), have also been reported (Table 1, Supporting Information).

New Class of Oxidative Decarboxylases. The crystal structures of human m-NAD-ME, pigeon c-NADP-ME, and *A. suum* m-NAD-ME show that the polypeptide backbone of malic enzymes has a different topology from that of the other oxidative decarboxylases (Figure 1A) (*12*, *18*, *23*, *24*). Therefore, the structure information establishes malic enzymes as a new class of oxidative decarboxylases.

Malic enzyme has an α/β structure. It belongs to an amino acid dehydrogenase-like family and a superfamily that contains the NAD(P)-binding Rossmann-fold domain. The core structure includes three layers of $\alpha/\beta/\alpha$ type, a parallel β-sheet of six strands in the order of 321456. The ME monomer was divided into four domains (A, B, C, and D) (Figure 1A) (*12*), and these domains behave mostly as rigid-bodies in the conformational transition between open and closed forms of the enzyme (Figure 1E and following text). Domain A contains residues 23−130[2] and is mostly helical (αA1 through αA6) (Figure 1A). Domain B consists of two segments of the polypeptide chain, residues 131−277 and 467−538 (Figure 1B), with domain C (residues 278−466) as an inserted cassette. Domain D, residues 539−573, contains one helix followed by a long extended structure that protrudes away from the rest of the monomer (Figure 1A).

Domain B contains a central, parallel five-stranded β-sheet (βB1 through βB5), which is surrounded by helices on both sides (αB1 through αB8) (Figure 1B). This β-sheet represents a new backbone-fold for a five-stranded parallel β-sheet. There is a short β-hairpin structure (βB2′−βB3′) between strand βB2 and helix αB2 in this domain (Figure 1B). Residues in this hairpin structure are highly conserved among malic enzymes, including the first phosphate-binding GXGXXG motif in malic enzymes, 168-GLGDLG-173. However, the residues in this motif are not involved in NAD$^+$ binding, although they are located near the active site of the enzyme.

Domain C has the dinucleotide-binding Rossmann fold, with the exception that strand three is replaced by a short antiparallel strand (βC2′, Figure 1C). In addition, there is an extra β-strand (βC7) at the C-terminal end of the domain, together with a β-hairpin insertion between βC6 and βC7. The NAD$^+$ cofactor in the active site is associated with this domain. The second dinucleotide-binding signature motif, 311-GAGEAA-316, is located between βC1 and αC1 in this domain and mediates the binding of the phosphates of the cofactor as in other Rossmann folds (Figure 1C). However, the amino acid conservation between this and other Rossmann-fold domains is very low, in the 15% range.

Open and Closed Forms of Malic Enzymes. The first structure of human m-NAD-ME, in a binary complex with NAD$^+$, is in an open form, as the active site region is fully

[2] To facilitate the comparisons of the sequences and structures of this large family of highly conserved enzymes, all the residues in these enzymes were numbered according to those in human m-NAD-ME, for which the first structural information was obtained on these enzymes. For pigeon c-NADP-ME, 21 should be subtracted from the corresponding numbers. For *Ascaris suum* m-NAD-ME, 14 should be added instead. When residues from other subunits are discussed, small letters are used to indicate the origin of the subunit (e.g., Trp572d denotes Trp572 from subunit d).

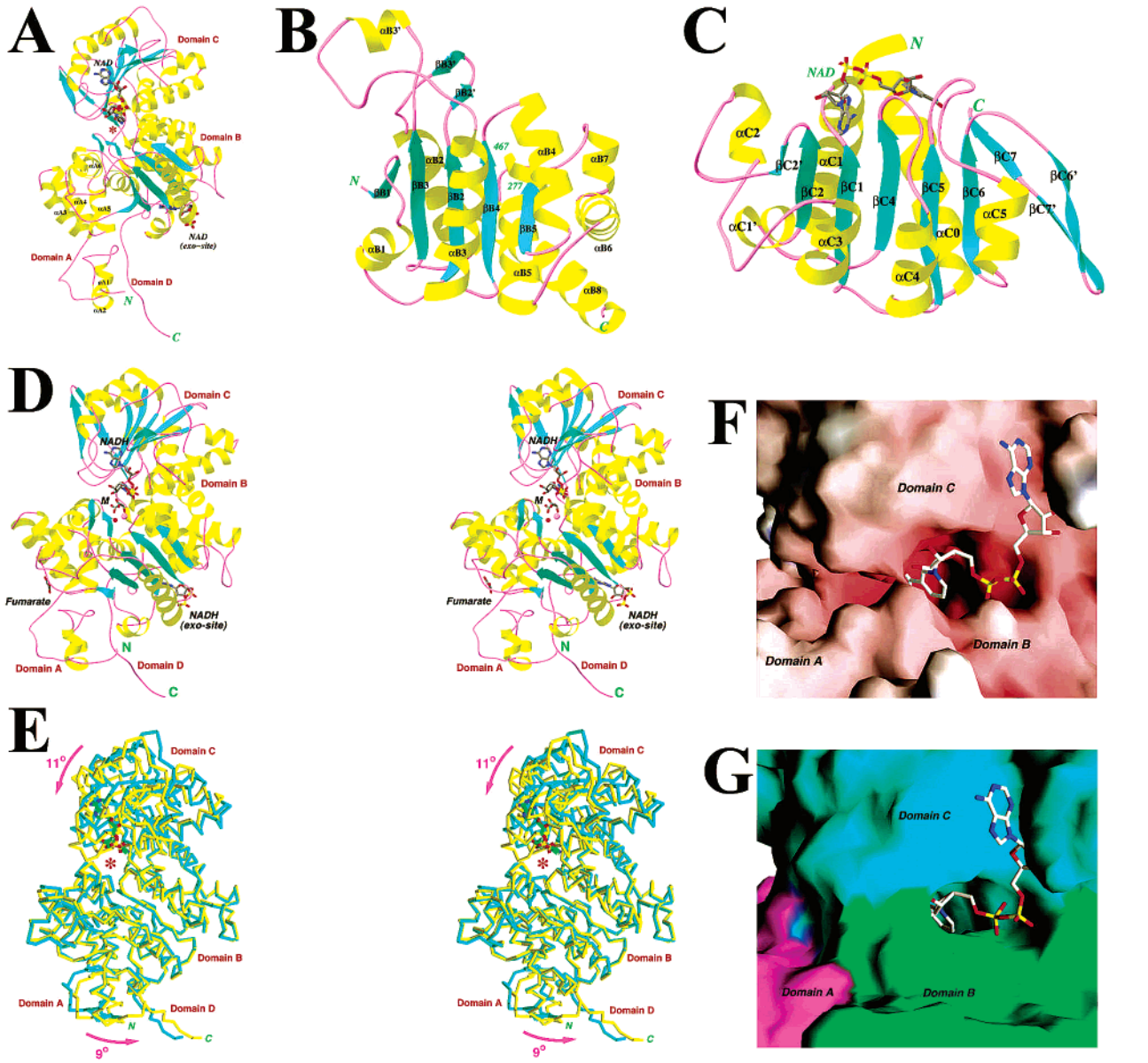

FIGURE 1: Structures of monomers of human m-NAD-ME. (A) The structure of m-NAD-ME in a binary complex with NAD^+, in open form I. The β-strands are shown in cyan, α-helices in yellow, and the connecting loops in purple. The four domains of the structure are labeled. The active site is indicated by the red star. Only the ADP portion of the NAD^+ molecule in the exo site is shown. (B) The structure of domain B, with a central parallel five-stranded β-sheet. (C) The structure of domain C, with a bound NAD^+ molecule. (D) The structure m-NAD-ME, in a pentary complex with NADH, malate (labeled as M), Mn^{2+} (pink sphere), and fumarate, in closed form II. (E) Overlap of the Cα traces of the binary, open form (in cyan) and pentary, closed form (in yellow) of m-NAD-ME, showing the large rigid-body movements of the domains. (F) Molecular surface of the binary complex, in open form I, near the active site, colored according to electrostatic potential. (G) Molecular surface of the pentary complex, in closed form II, near the active site, colored by the three domains.

exposed to the solvent (Figure 1F) (*12*). Upon binding the divalent cation and the substrate (malate or pyruvate) or substrate-analogue inhibitors (oxalate, tartronate, or ketomalonate), the enzyme undergoes a large conformational change (*20*−*22*). In this closed form of the enzyme, the divalent cation and the substrate or inhibitor are shielded from the solvent (Figure 1G). The closed form of the enzyme is likely the catalytically competent conformation, while the open form may be required for substrate binding and product release. Therefore, it is possible that most malic enzymes can undergo the open-closed transition during catalysis.

The closure of the active site is mediated by the rigid-body movement of domain C with respect to domain B, including a relative rotation of 10.6° between the two domains (Figure 1E) (*20*). Interestingly, residues in domains A and D also undergo a rigid-body shift, with a rotation of 9.2° (Figure 1E). This causes a reorganization of the tetramer of human m-NAD-ME. The movements of domain C and domains A and D are independent of each other. In the structure of human m-NAD-ME in a ternary complex with NAD^+ and Lu^{3+} (*19*), the movement in domains A and D is observed, but the active site remains open. Therefore, it appears that human m-NAD-ME can exist in two open forms and possibly two closed forms as well.

Kinetically, Lu^{3+} is a competitive inhibitor with respect to Mn^{2+} (*19*). The dynamic quenching constants of the intrinsic fluorescence for the metal-free and Lu^{3+}-containing enzymes are quite different, indicating the conformational

differences between the two enzyme forms. The secondary structure of these two enzyme forms, on the other hand, remains unchanged. Replacement of the catalytically essential Mn^{2+} by other metal ions (Zn^{2+}, Cu^{2+}, or Fe^{2+}) leads to a slow conformational change of the enzyme and consequently alters the geometry of the active site (*26*). The transformed enzyme conformation, however, is unfavorable for catalysis. Both the chemical nature of the metal ion and its correct coordination in the active site are essential for catalysis.

The Lu^{3+}-induced isomerization was completely reversible. The Lu^{3+}-inhibited activity can be fully reactivated and the dynamic quenching constant completely returned to that of the open form by Mn^{2+} (*27*). This finding indicates that the tertiary structure of the E-NAD^+-Mn^{2+} complex is indistinguishable from the E-NAD^+ open form by the fluorescence quenching analysis. The open form transformed to the closed form only after substrate binding. Lu^{3+}, on the other hand, transformed the open form into a catalytically inactive form, which may not be a physiologically relevant structure. Excess Mn^{2+} could replace Lu^{3+} in the metal-binding site and convert the inactive form back to the open form and may be an open form II, which is not obviously distinct from the open form I in the routine biophysical probe fluorescence quenching analysis (*27*).

Tetramer of the Enzyme. The tetramer of malic enzymes obeys a 222 point-group symmetry, with each monomer having essentially the same environment (Figures 2A and 3A). The four monomers are positioned at the four corners of a square, an arrangement first observed in the electron microscope images of pigeon liver malic enzyme (*28*). The dimensions of the tetramer are about 110 × 110 × 55 Å, consistent with electron microscopy and solution light scattering studies (*16*, *28*).

The tetramer is a dimer of dimers, with intimate contacts at the dimer interface, whereas the association of the two dimers is weaker (Figures 2A and 3A). This is in agreement with the biochemical studies showing that pigeon c-NADP-ME exists in a monomer−dimer−tetramer equilibrium in solution (*29*). Mutation at some positions near the N-terminus, located at the dimer interface, affects the quaternary structure (*30*, *31*). The dimer interface involves residues from domains A and B of the monomer. Helices αA3 and αA4, and their 2-fold symmetry mates, form a four-helical bundle at this interface (Figure 2A). Interactions at the tetramer interface are primarily mediated by the long, extended segment at the C-terminus of the malic enzyme monomer (domain D) (Figure 1A). It latches onto the other dimer of the tetramer and interacts with both of its monomers (Figures 2A and 3A). The side chain of residue Trp572 is completely buried at this tetramer interface. Mutation of this Trp to Phe has a tremendous effect on the quaternary structure of the enzyme (*32*). Besides the C-terminal segment, residues 541−544 also make a contribution to the formation of the tetramer in human ME (Figure 2C) (Table 2, Supporting Information).

There are substantial differences between pigeon c-NADP-ME and human m-NAD-ME in the subunit interfaces (Table 2, Supporting Information). The major interactions between subunits are hydrophobic interactions in both enzymes (Figure 3C). Hydrogen bonding also contributes significantly in the subunit association. Three salt bridges in c-NADP-ME, one in Glu27a/Lys23b, and two in Arg74a/Asp80b pairs are absent in the m-NAD-ME. Two cation−π interactions, absent in c-NADP-ME, are found in m-NAD-ME between Arg484d and Tyr543a. Other interchain cation−π interactions greater than 3.5 Å but within 6 Å include Arg128a/Tyr84b and Lys26a/Trp150b pairs in the A−B dimer interface.

The tetramer interface is due to interactions between subunits A and D as well as A and C. The former (A/D) interaction can be divided into three groups (Figure 3C). The first is due to the contact of subunits A and D at the exo site, which involves the protruding of Tyr543a into subunit D forming a cation−π interaction between Tyr543a-CD2 and Arg484d-CZ. c-NADP-ME lacks intimate interaction in this area. Tyr543a in c-NADP-ME points to subunit A itself, almost 180° different in direction as compared to Tyr543a in the m-NAD-ME. The other two areas involve interactions in the dimer interface area and the extension of the C-terminus domain D into the other dimer (Table 2, Supporting Information).

There are large differences in the organization of the tetramer of human m-NAD-ME between the binary complex with NAD^+ (an open form, Figure 2A) and the pentary complex with NADH/malate/Mn^{2+}/fumarate (a closed form, Figure 2D) (*12*, *20*, *22*). This reorganization is mediated by rigid-body movements of residues in domains A and D, as described in the previous section (Figure 1E). Both the dimer and the tetramer interfaces are affected by this reorganization.

On the basis of current structural information on the human m-NAD-ME, its tetramers may exist in one of the four states (and additional states may also be possible). These four states include open forms I and II and closed forms I and II (Figure 2A−D). The closure of the active site, mediated by the movement of domain C, distinguishes the open and closed forms. The reorganization of the tetramer, mediated mostly by the rigid-body movements in domains A and D, distinguishes the two open or two closed forms. The structure of human m-NAD-ME in the NAD^+ binary complex represents open form I (Figure 2A), whereas the structure of the ternary NAD^+/Lu^{3+} complex may be open form II (Figure 2B). The structures of the quaternary and pentary complexes of human m-NAD-ME all correspond to closed form II (Figure 2D). The closed form I (Figure 2C) has yet to be observed experimentally, and it might be unstable.

It is not known whether other malic enzymes can also assume two open and two closed forms. The quaternary complex of pigeon c-NADP-ME is in closed form II (*23*), and it would be of interest to determine the conformation of the open form(s) of this enzyme. The binary complex of *A. suum* m-NAD-ME with NAD^+ is in open form I (*24*). The closed forms of the *ascaris* ME are yet to be determined.

The two open forms for human m-NAD-ME might be related to its allosteric activation by fumarate (*21*). Fumarate is bound at the dimer interface, but the open form I structure is not compatible with fumarate binding (see next). The *A. suum* m-NAD-ME can also be activated by fumarate (*33*). The allosteric site where tartronate is bound is assumed to be the activator site for fumarate (*25*). In this regard, it is interesting that the binary complex of this enzyme, in the absence of fumarate, is also in open form I. Therefore, the open form I structure might be linked to allosteric regulation of some of these enzymes, while most other malic enzymes can only assume open form II and closed form II.

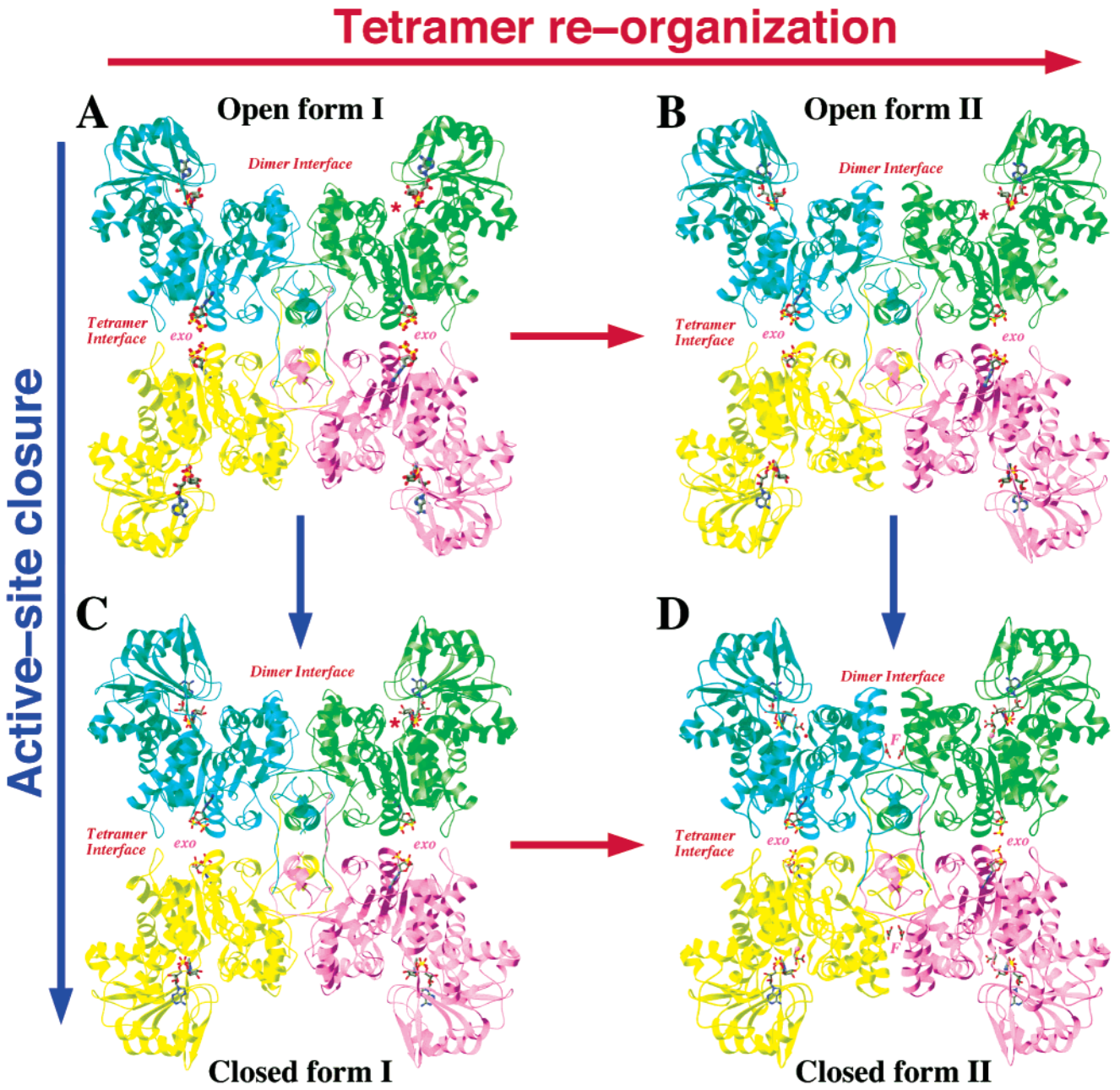

FIGURE 2: Tetramer of malic enzymes. Schematic drawing of the tetramer of human m-NAD-ME in (A) open form I, (B) open form II, (C) closed form I, and (D) closed form II. The monomers are colored in green, cyan, yellow, and purple, respectively. The active site is indicated by the red star. The hypothetical closed form I has not been observed experimentally yet.

The four active sites of the tetramer are separated from each other by about 60 Å and from the dimer or tetramer interface by about 32 Å (Figures 2A and 3A). Most malic enzymes have simple, hyperbolic kinetics with respect to their substrates suggesting that the four active sites are functioning independently. However, human and *A. suum* m-NAD-ME exhibit cooperative behavior with respect to the substrate malate, but the sigmoidal kinetics is abolished in the presence of the fumarate activator (*33*−*35*). The binding of either malate or fumarate may induce the transition from open form I to open form II in the dimer of these enzymes, and this transition may be the molecular basis for the observed cooperativity. An anticooperative behavior has been reported for the pigeon c-NADP-ME (*36*, *37*), but no asymmetry in the tetramer is apparent from the structural studies (*23*).

Comparison of ME from Various Sources. As shown in Figure 3B, the active site of ME constitutes a major conserved region. Some of the subunit contacting regions are also conserved among ME (Figure 3C). The amino acid sequences around the metal-binding site are highly conserved. The direct metal ligands, Glu255, Asp256, and Asp279, are identical among all malic enzymes, from bacteria to humans (Figure 3D). The catalytic mechanism should be essentially the same for all malic enzymes.

Figure 3E shows the superimposed crystal structures of some resolved malic enzymes. The overall structure of human m-NAD-ME, pigeon c-NADP-ME, and *A. suum* m-NAD-ME are similar. The alignment regions are residues 21−573 for the closed form human m-NAD-ME (1OX2), 23−573 for the open form human m-NAD-ME (1QR6), 23−578 for the pigeon c-NADP-ME (1GQ2), and 12−563 for

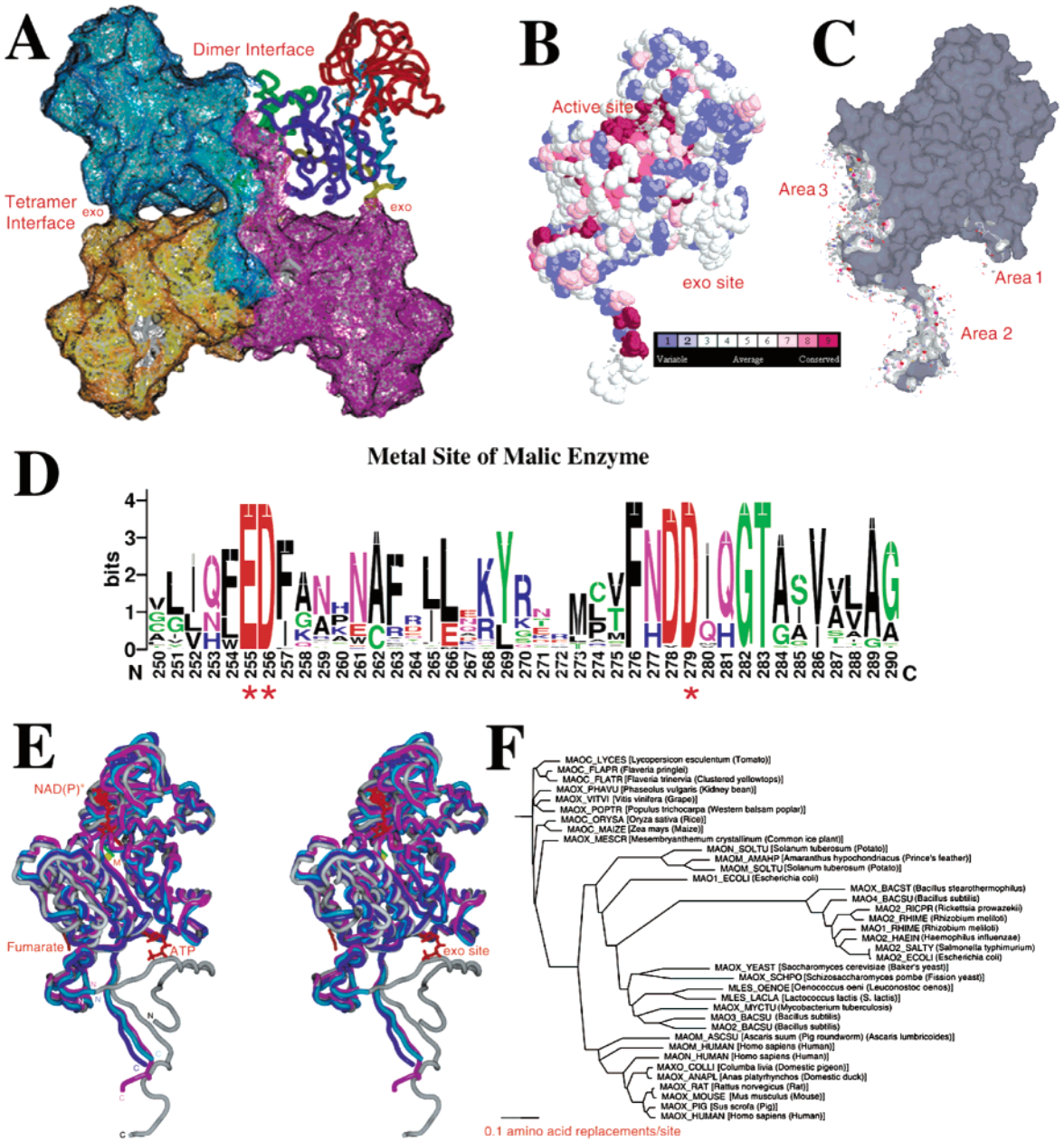

FIGURE 3: Comparison of ME structures. (A) Quaternary structural features of malic enzyme. The four domains of subunit B are shown as a worm model in green, blue, red, and yellow, respectively. (B) Functional and conserved regions of ME. The discrete conservation color scheme used for visualization is based on the continuous conservation scores. The conserved regions are shown in violet and variable region in blue with a visual color key provided (*61*), in which color grades (1−9) are assigned. (C) Surface of the ME monomer showing the subunit contacting regions. White or light areas denote hydrophobic contacts between subunits. Magenta areas denote putative hydrogen-bond contacts. The nearby residues are shown with a stick model in CPK color. Generated with Protein Explorer v1.982b (*62*). (D) Sequence logos of ME around the metal-binding site. Amino acid sequences of ME were searched for alignment by ConSurf (*61*), and the result is expressed by sequence logos with error bars shown (*63*). The metal-binding ligands, Glu255, Asp256, and Asp279 (red stars), are strictly identical among all ME. Conservation of some putative second sphere hydrophobic amino acid residues is also evident in this figure. Color codes for the amino acids are as follows: blue for basic residues (Lys, Arg, and His), red for acidic residues (Asp and Glu), violet for amide residues (Asn and Gln), green for other neutral/polar residues, and black for hydrophobic residues. (E) Stereo model showing the superimposition of the crystal structures of human m-NAD-ME (1QR6, blue and 1OX2, turquoise), pigeon c-NADP-ME (1GQ2, magenta), and *A. suum* m-NAD-ME (1LLQ, gray). The structures of 1OX2 and 1GQ2 are those of the closed form and those for 1QR6 and 1LLQ are the open form. The yellow ball denotes the manganese ion. (F) Phylogenetic tree of ME from various sources. Thirty-seven ME sequences from Swiss-Prot database (release 41.16) were analyzed by the ConSurf (*61*). Each entry name is followed by its accession number: Mao1 Bacsu (P54572); Mao1 Ecoli (P26616); Mao1 Rhime (O30807); Mao2 Bacsu (P45868); Mao2 Ecoli (P76558); Mao2 Haein (P43837); Mao2 Rhime (O30808); Mao2 Ricpr (Q9ZDF6); Mao2 Salty (Q9ZFV8); Mao3 Bacsu (O34389); Mao4 Bacsu (O34962); Maoc Flapr (P36444); Maoc Flatr (P22178); Maoc Lyces (P37222); Maoc Maize (P16243); Maoc Orysa (P43279); Maom Amahp (P37224); Maom Ascsu (P27443); Maom Human (P23368); Maom Soltu (P37221); Maon Human (Q16789); Maon Soltu (P37225); Maox Anapl (P28227); Maox Bacst (P16468); Maox Colli (P40927); Maox Human (P48163); Maox Mescr (P37223); Maox Mouse (P06801); Maox Myctu (P71880); Maox Phavu (P12628); Maox Pig (Q29558); Maox Poptr (P34105); Maox Rat (P13697); Maox Schpo (P40375); Maox Vitvi (P51615); Maox Yeast (P36013); Mles Lacla (Q48662); and Mles Oenoe (Q48796).

the *A. suum* m-NAD-ME (1LLQ) (*24*). The backbone traces are similar in all malic enzymes with small local conformational differences, which reflect the structural basis of the different properties observed in the catalysis of substrate or cofactors specificities.

Among the structural differences of ME is the length of domain D (Figure 3E). Pigeon c-NADP-ME has a C-terminus seven residues longer than the human m-NAD-ME. The *A. suum* enzyme, on the other hand, has both long C- and N-termini. Because of these differences, the ME from different species have various strengths in the quaternary structure. At neutral pH, c-NADP-ME exists as tetramer, which sediments as a single species with a sedimentation coefficient of approximately 10 S. m-NAD-ME, on the other hand, exists as a mixture of tetramer and dimer under the same conditions (*38*). It is interesting to note that both $NAD(P)^+$- and $NADP^+$-dependent ME from *Rhizobium melitoti* and other Gram-negative bacteria are chimeric proteins with a large phosphotransacetylase-like domain of approximately 320 amino acid residues at the C-terminus. Mutants without this C-terminal region retain ME activity but are unable to oligomerize into the native state (*39*). In human m-NAD-ME, the allosteric regulated ATP and fumarate are bound at the tetramer and dimer interfaces, respectively. A single mutation at the exo ATP site of Arg542 to alanine will produce dimeric mutants R542A (*38*).

From the 37 available amino acid sequences of ME, a phylogenetic tree of ME was built. Five clusters of ME are grouped (Figure 5F). Between the plant kingdom (upper part in Figure 5F) and the animal kingdom (lower part) are prokaryotic bacteria and eubacteria. Two malolactic enzymes from lactic acid bacteria (*Oenococcus oeni* and *Lactococcus lactis*) catalyzing the degradation of L-malate to CO_2 and lactate with concomitant reduction of NAD^+ to NADH also belong to the malic enzyme family.

Dual Functional Roles of Metal Ion in the Mechanism of ME. The enzyme needs an essential divalent metal ion (Mn^{2+} or Mg^{2+}), which plays dual functional roles in catalysis and in structural stability. The three metal ligands Glu255, Asp256, and Asp279 are 2.43, 2.19, and 2.23 Å, respectively, to the manganese ion, forming a reaction core. Among other amino acid residues within 7 Å from the metal ion are many hydrophobic amino acid residues (i.e., Phe254, Phe257, Ile166, Leu167, and Ile179). These amino acid residues form a second sphere for the catalytic metal ion and the other polar groups in the active center and ensure an optimal environment for substrate binding and catalytic reactions (*40*). Alteration of these residues, even indirectly, might affect the catalytic efficiency. For example, the mutation of Phe257 to leucine contributes −2.19 kcal/mol for the coupling energy between Phe257 and Asp162 on the metal binding (*41*).

The importance of hydrophobicity in the second sphere of the metal binding site is enforced by the finding that the change of Phe257 to a less hydrophobic alanine (F257A) results in loss of 2.51 kcal/mol for the metal binding energy. Substitution of Phe257 by the more hydrophobic leucine (F257L), on the other hand, can restore most of the lost binding energy (1.41 kcal/mol) (*41*). The functional role of all these amino acid residues in the putative second sphere of the metal site will, however, have to await further study.

The c-NADP-ME is reversibly dissociated under acidic environment or in the presence of a chemical denaturant. The dissociated monomers are easily polymerized. Manganese ion provides full protection against polymerization (*32*, *42*). The native enzyme changes to a supra-active conformation at 1 M urea concentration. The sedimentation coefficient of this form is slightly decreased when compared to the native state. All these data support a metal ion-induced open form II that has a different conformation with the open form I. In the absence of Mn^{2+}, the partially unfolded tetramer, presumably in the open form I, quickly dissociates to a partially unfolded monomer when the urea concentration increases to 2 M. In the presence of Mn^{2+}, it will remain as a partially unfolded tetramer. When the urea concentration is further increased to 3−5 M, the exposed hydrophobic site of the partially unfolded monomer induces polymerization. Mn^{2+} can delay this polymerization up to 5 M urea. Eventually, all aggregates will be dissolved in urea higher than 6 M to give the denatured monomer. However, since the enzyme activity is not restored by dilution, the unfolding is not reversible. It seems that, under physiological concentration of manganese or magnesium concentration, ME exists as the metal ion-containing open form II, which is resistant to aggregation.

There are a total of three to four Trp in each subunit of ME, distributed in different structural domains of the enzyme. These Trp are ideal intrinsic chromophores to study the local conformational changes of ME. Several Trp mutants have been constructed to access different structural domains of the pigeon c-NADP-ME (*42*). Substitution of a single tryptophanyl residue, Trp572, by phenylalanine renders a loss of protective ability of Mn^{2+} against the polymerization (*42*). The Trp572 residue from subunit A is located in a deep, hydrophobic pocket from the neighboring subunit and is involved in the tetramer interaction. The crystal structure of the enzyme shows that there are some nearby histidyl residues. Protonation of these histidyl residues at a lower pH can affect the binding of the Trp572 residue in the tetramer interface, which in turn, destabilizes the tetramer interface (*29*). The tetrameric structure is essential for the overall structural stability of ME.

Active Site of the Enzyme and Substrate/Inhibitor Binding Modes. The active site of malic enzyme is located in a deep cleft at the interface between domains B and C of each molecule (Figure 1G) together with several residues from domain A (mostly from helix αA6, Figure 4A). The amino acid residues in the active site region are generally highly conserved among the malic enzymes, supporting their importance in substrate binding and/or catalysis (Figure 3D). The active site residues can be roughly divided into four categories: (1) divalent cation-binding residues (Glu255, Asp256, and Asp279); (2) substrate-binding residues (Thr113, Pro114, Val116, Arg165, Ile166, Leu167, Ile179, Asn421, and Pro422); (3) $NAD(P)^+$ cofactor binding residues (310−316, Asp345, 346, Arg354, 362, Ala393, and Asn467); and (4) catalytic residues (Tyr112 and Lys183). The structural roles of residues binding the divalent cation and substrate/inhibitor are described here. Residues binding $NAD(P)^+$ will be described in the section on cofactor selectivity, whereas the residues Tyr112 and Lys183 will be discussed in the section on the catalytic mechanism of these enzymes.

The divalent cation is bound deep in the active site cleft (Figure 4A) and is octahedrally coordinated by six oxygens, one each from the side chain carboxylate groups of Glu255,

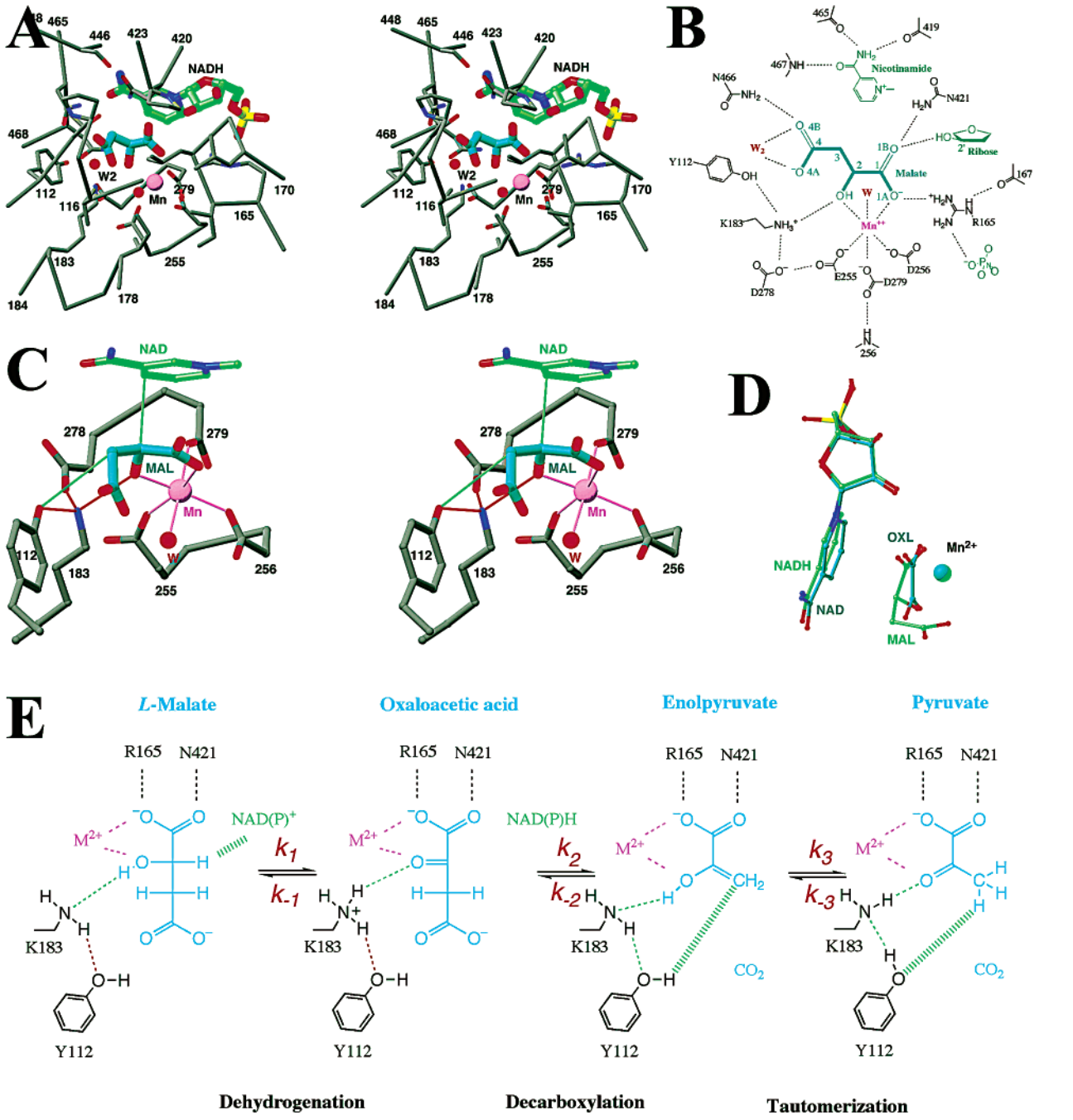

FIGURE 4: Active site of malic enzymes. (A) Residues of human m-NAD-ME near the active site of the enzyme, shown in gray for carbons. The malate molecule is shown with the carbon atoms in cyan and the NAD^+ molecule in green. The Mn^{2+} ion is shown as a purple sphere and the water molecules in red. (B) Schematic drawing of the polar interactions in the active site of human m-NAD-ME. (C) Close-up of the active site of human m-NAD-ME, showing the hydrogen-bonding interactions for the Lys183 side chain. The hydride transfers between the C2 atom of malate and the C4 atom of nicotinamide, and the proton transfer between Tyr112 and C3 atom of the substrate, are indicated in green. (D) Comparison of the binding modes of NAD^+, oxalate, and Mn^{2+} in the quaternary complex with those of NADH, malate, and Mn^{2+} in the pentary complex. (E) A possible catalytic mechanism for malic enzymes. The other proton on the Lys183 side chain is hydrogen bonded to Asp278 throughout the reaction cycle.

Asp256, and Asp279, two from the substrate or inhibitor, and one from a water molecule (Figure 4C). The identification of Asp279 as a ligand to the cation is in agreement with the previous biochemical studies on the pigeon and *A. suum* malic enzymes (*43*−*45*).

By studying the dead-end NADH/malate and NAD^+/pyruvate complexes, the bound conformations of the malate and pyruvate substrate molecules have also been determined (*22*). Malate is bound in the active site such that the C2 hydroxyl is essentially in the same plane as the C1 carboxylate group (Figure 4A). The C2 hydroxyl and one of the C1 carboxylate oxygen atoms are ligands to the divalent cation (Figure 4C). Malate is also involved in a large network of hydrogen-bonding and ionic interactions with the enzyme (Figure 4B). The carboxylate oxygen atom (O1A) that is ligated to the divalent cation also has ionic interactions with the side chain guanidinium group of Arg165, whereas the other carboxylate oxygen atom (O1B) is hydrogen bonded to the side chain amide of Asn421 and the 2′-hydroxyl of the nicotinamide ribose.

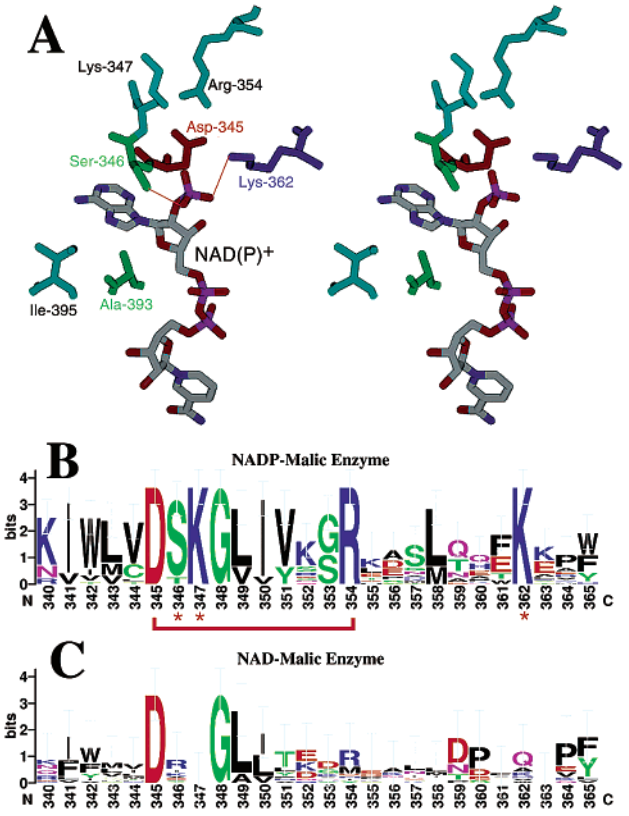

FIGURE 5: Possible molecular mechanism for cofactor selectivity. (A) Structure features of pigeon c-NADP-ME near the 2′-phosphate of $NADP^+$. The interactions between 2′-phosphate of $NADP^+$ and Ser346 and Lys362 are highlighted with red lines. (B) Sequence logos of ME around the nucleotide-binding site of NADP-ME. ME sequences near the binding site for the 2′-phosphate of $NADP^+$. The amino acid residues responsible for the nucleotide specificities are marked with red stars. The Asp345:Arg354 ion pair is highlighted. (C) Sequence logos of ME around the nucleotide-binding site of NAD-ME. In panels B and C, the color codes for the amino acids are as follows: blue for basic residues (Lys, Arg, and His), red for acidic residues (Asp and Glu), violet for amide residues (Asn and Gln), green for other neutral/polar residues, and black for hydrophobic residues.

The C4 carboxylate group of malate is out of the plane defined by the C1, C2, O2, and C3 atoms (Figure 4C). It is within the hydrogen-bonding distance to the side chain of Asn466, the water ligated to the cation, and a second water molecule (Figure 4B). The C3 atom of malate, on the other hand, does not have close contacts with atoms in the enzyme (Figure 4A).

The bound conformation of the oxalate molecule is consistent with its role as an analogue of the enolpyruvate transition-state intermediate as well as the pyruvate product (*20*, *22*). Structural comparison between pyruvate and malate shows that the C2 atoms of the two molecules are separated by about 0.6 Å (Figure 4D), partly due to the difference in the hybridization state of this atom (sp^2 vs sp^3) in the two compounds (*22*).

The active site also contains several hydrophobic residues, and the majority of them do not have direct interactions with the substrate (Figure 4A) but instead help shield the active site region from the solvent in the closed form. Interestingly, the two prolines in the active site (Pro114a and Pro422c) are both in the cis conformation and form a lid over the active site (Figure 4A).

The structural information is generally consistent with the observations from previous biochemical studies on these enzymes. Chemical modification of an Arg residue in pigeon and maize malic enzyme disrupted malate binding without affecting $NADP^+$ binding (*46*, *47*). This is likely Arg165 in the active site (Figure 4A). Modification of tyrosyl residue, probably Tyr112, with tetranitromethane also affects malate binding (*48*). The fluorescent affinity label 3-aminopyridine adenine dinucleotide phosphate dialdehyde (oAADP) specifically binds the enzyme at the nucleotide-binding site and forms a Schiff's base with lysyl residue (*49*). The labeled position, not proved then, very likely is the Lys362. Covalent modification of the side chain of Cys120 by the substrate-analogue bromopyruvate can also disrupt malate binding (*36*, *50*). However, Cys120 is more than 10 Å away from the active site, suggesting an indirect effect (*12*).

Possible Catalytic Mechanism. The catalysis by malic enzymes generally proceeds in three steps—dehydrogenation of malate to produce oxaloacetate (k_1), decarboxylation of oxaloacetate to produce enolpyruvate (k_2), and finally tautomerization of enolpyruvate to produce pyruvate (k_3) (Figure 4E) (*51*). The divalent cation at the optimal position helps catalyze all the steps of the reaction, which explains its requirement for catalysis by malic enzymes. Trivalent lanthanide ions can bind to the enzyme at this site and potently inhibit the catalysis by both human and pigeon malic enzymes (*19*, *26*, *27*).

For the oxidative decarboxylation of malate, a general base is needed to extract the proton from the C2 hydroxyl group to initiate the dehydrogenation reaction (k_1) (Figure 4E). For the tautomerization reaction (k_3), a general acid is needed to protonate the enolpyruvate intermediate at the C3 position, and a general base is needed to extract the proton from the C2 hydroxyl of this intermediate (Figure 4E). It has been proposed, based on kinetic and mutagenesis studies, that Asp279 is the general base and that Lys183 is the general acid (*45*, *52*). The structural information suggests, however, that this is unlikely. Asp279 is a ligand to the cation and is not positioned correctly to function as the general base, while the Lys183 side chain is more than 3.6 Å from the C3 atom of pyruvate (*22*).

On the basis of the structures of human m-NAD-ME in complex with malate and pyruvate, Lys183 has been identified as the general base and Tyr112 as the general acid (*22*). The Lys183 side chain is hydrogen bonded to the C2 hydroxyl (or carbonyl) of the substrate and the side chains of Tyr112 and Asp278 (Figure 4C). The Lys183 side chain, in the neutral form, is perfectly positioned to extract the proton from the C2 hydroxyl of malate (Figure 4E). In the decarboxylation reaction (k_2), Lys183 functions as a general acid and donates its proton to the C2 hydroxyl to produce the neutral enol. For the tautomerization of enolpyruvate (k_3), Tyr112 donates a proton to the C3 position, while Lys183 extracts the proton from the C2 hydroxyl (Figure 4E). During this process, the proton shared between the two residues changes its position to maintain both of them in the neutral state (Figure 4E). Therefore, Tyr112−Lys183 functions as a general acid−base pair in this reaction.

Mutation of the Lys general base has large effects on the catalytic activity of malic enzymes (*20*, *52*, *53*). For example, mutation of this Lys to Ala in the *A. suum* malic enzyme produces a 130 000-fold decrease in the V_{max} of the overall

reaction (*52*). In comparison, mutation of the Tyr general acid has smaller effects on the reaction, with the Tyr to Phe mutant having about 1500-fold lower k_{cat} for the oxidative decarboxylation of malate (*20*, *52*). It is likely that the protonation of enolpyruvate (k_3) is not a rate-determining step of the forward reaction. It may also be possible that a water molecule is recruited into the active site of this mutant and partially rescues its catalytic activity. It would be interesting to characterize the effects of Tyr112 mutation on the rate of the reverse reaction, the reductive carboxylation of pyruvate ($k_{-3} - k_{-1}$).

In the complex with malate, the proton on the C2 atom is pointed toward the C4 atom of the nicotinamide ring of NAD^+, with a hydride transfer distance of about 2 Å. This explains the stereospecificity of malic enzyme for L-malate, as D-malate cannot adopt the same binding mode (*12*). Moreover, the structure predicts a hydride transfer to the *A* face of the nicotinamide ring for malic enzymes, consistent with the experimental observations (*54*). It would be interesting to compare the substrate binding modes between ME and tartrate dehydrogenase, which catalyzes the oxidative decarboxylation of D-malate (*55*).

$NAD(P)^+$ Binding and Cofactor Specificity. The $NAD(P)^+$ cofactor in the active site is associated with domain C (Figure 1C), at a position similar to that of the dinucleotide in other Rossmann-fold domains. The adenine ring is on the surface of the protein and positioned between the side chains of residues 346 and 393, but the N1 and N6 atoms of the adenine base are not specifically recognized by the enzyme. The nicotinamide ring is in the anti conformation. Residue Gly446, strictly conserved among malic enzymes, is located close to the amide group on this ring. Mutation of this residue to Asp in the *Schizosaccharomyces pombe* malic enzyme inactivated the enzyme (*56*). A syn conformation for the nicotinamide ring was observed in the quaternary complex of *A. suum* m-NAD-ME with NADH, tartronate, and Mg^{2+} in open form I (*25*).

Malic enzymes have highly conserved amino acid sequences but have distinct specificities toward the dinucleotide cofactor. Some malic enzymes can only use NAD^+ as the cofactor, while others can only use $NADP^+$. Human m-NAD-ME is among the few malic enzymes that has dual-specificity and can use either NAD^+ or $NADP^+$ but prefers NAD^+ under physiological conditions (*57*). The molecular basis for cofactor selectivity by these and other enzymes is still poorly understood.

Earlier studies with other enzymes have revealed two major determinants for cofactor specificity (*58*, *59*). First of all, an Asp residue near the end of the second strand of the Rossmann fold generally indicates NAD^+ preference, as it recognizes the 2′-hydroxyl group on the ribose and cannot tolerate the phosphate group in $NADP^+$. Second, enzymes that contain a GXGXXG dinucleotide-binding motif generally prefer NAD^+, whereas those with a GXGXXA motif generally prefer $NADP^+$. However, malic enzymes appear to disobey both of these rules. An Asp residue (Asp345) is conserved among all malic enzymes at the end of the second strand (βC2) in domain C. Moreover, most malic enzymes from animals contain the GXGXXA motif, whereas those from lower organisms contain the GXGXXG motif, irrespective of their cofactor specificity. The structures show that the Asp345 residue is pointed away from the ribose, forming ion-pair interactions with Arg354 (Figure 5A,B). This may explain why some malic enzymes can use $NADP^+$ as the cofactor even with a conserved Asp at this position.

The structure of the quaternary complex of pigeon c-NADP-ME suggests a possible molecular mechanism for the $NADP^+$ specificity of this enzyme (*23*). The 2′-phosphate group of $NADP^+$ is placed on the surface of the enzyme and interacts with residues Ser346 and the side chain ammonium group of Lys362 (Figure 5A). These two residues are conserved among the $NADP^+$-dependent malic enzymes (Figure 5B). Several other residues near the 2′-phosphate group also have variations between $NADP^+$- and NAD^+-dependent malic enzymes (Figure 5B,C), although the mutation of Lys347, conserved among $NADP^+$-dependent malic enzymes, has little impact on the K_m for $NADP^+$ of c-NADP-ME (*53*). This side chain does not directly contact the 2′-phosphate group (Figure 5A). Mutation of Lys362, on the other hand, has a tremendous effect on the nucleotide binding on c-NADP-ME. The K362A mutant of pigeon c-NADP-ME has a 70-fold increase in the K_m for $NADP^+$ (*53*). The $(k_{cat}/K_{m,NADP})/(k_{cat}/K_{m,NAD})$ ratios are 0.51 and 31, respectively, for the mutant K362D and K362Q of c-NADP-ME as compared to the value of 7390 and 0.11, respectively, for the WT pigeon c-NADP-ME and human m-NAD-ME (Kuo, C. C., Chang, G. G., and Chou, W. Y., unpublished results). Residue 362 is Gln in human m-NAD-ME. It would be interesting to determine whether the Q362K mutant of human m-NAD-ME would prefer to utilize $NADP^+$ as the cofactor.

Binding Site for the Allosteric Activator Fumarate. The catalytic activity of human and *A. suum* m-NAD-ME is activated by fumarate (*33*−*35*). The binding site of fumarate in human m-NAD-ME has been located (*21*). An equivalent binding site may also exist in *A. suum* m-NAD-ME, based on the structure of this enzyme with tartronate bound at this site (*25*). The regulation of human m-NAD-ME is consistent with its role in the metabolism of glutamine for energy production, as fumarate is the product of the previous step of this pathway while ATP is the ultimate product of this energy metabolism (*12*). On the other hand, the c-NADP-ME isoform is mostly involved in generating NADPH for fatty acid synthesis; therefore, it is not subject to regulation by fumarate or ATP.

The fumarate-binding site is located at the dimer interface (Figures 2D and 3E), about 30 Å from the active site, confirming that fumarate functions through an allosteric mechanism (*21*). The binding pocket is on the surface of domain A of one monomer (Figures 1D and 6A). One carboxylate group of fumarate has bidentate ion-pair interactions with the side chain of Arg91, and the other carboxylate is in a mono-dentate ion pair with Arg67. Residues 123−130 from the other monomer of the dimer, in the linker between domain A and domain B, cover this binding pocket. Mutagenesis studies with Arg67 and Arg91 residues in human m-NAD-ME confirm their importance in fumarate binding (*21*). Both residues are conserved in *A. suum* m-NAD-ME (Figure 6B) and show similar interactions with the bound tartronate (*25*). Mutation of Arg91 in *A. suum* m-NAD-ME to alanine results in a decrease in both V/K_{malate} and V/K_{Mg}, and the mutant lost its fumarate activation property (*60*). However, both Arg67 and Arg91 are also conserved among many other malic enzymes (Figure 6B),

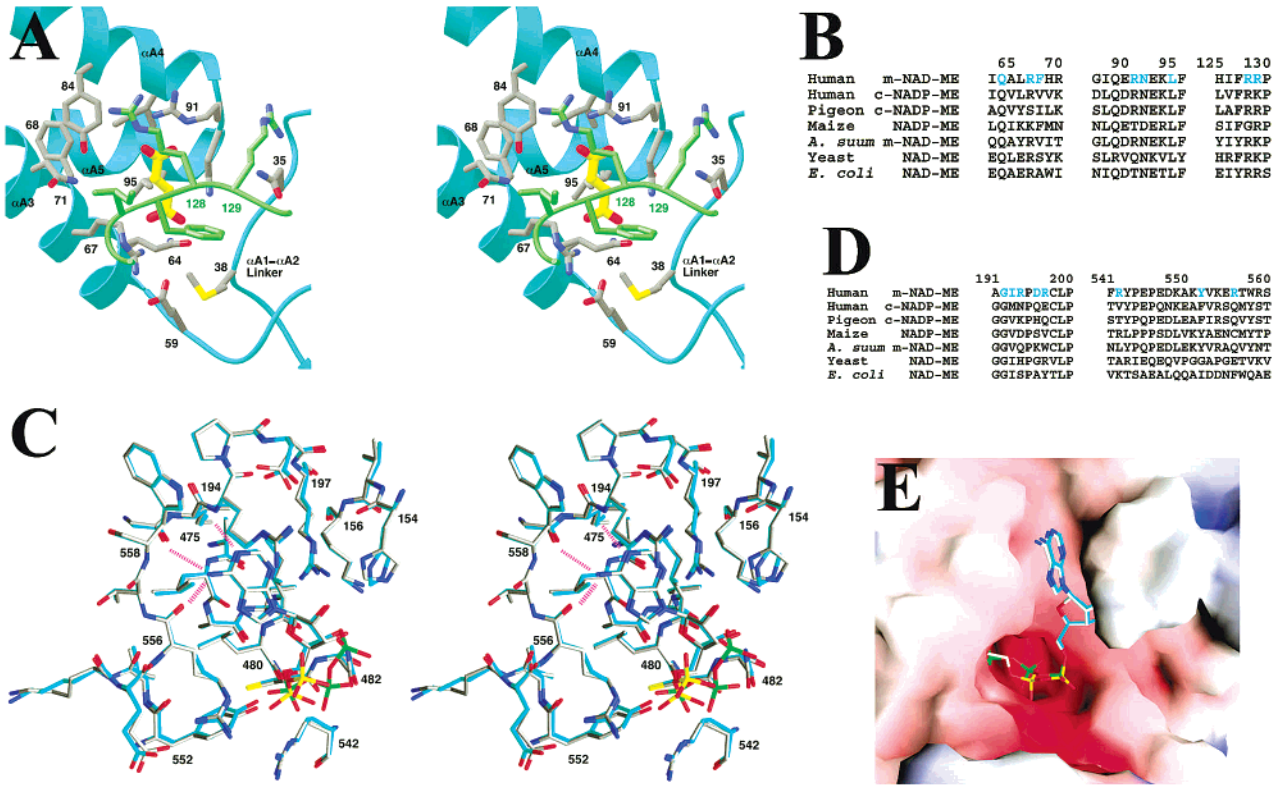

FIGURE 6: Binding sites for ATP and fumarate in human m-NAD-ME. (A) The binding of fumarate (in yellow for carbon atoms) to the allosteric site in the dimer interface (in cyan and green for the two monomers). (B) Sequence alignment of residues in the fumarate-binding site. Residues that interact with fumarate are shown in cyan. (C) Comparison of the binding modes of ATP (in cyan for carbon atoms) and the ADP portion of NAD^+ (in gray) to the exo site (in cyan for carbon atoms). The phosphorus atoms of ATP are shown in green and those of NAD^+ in yellow. (D) Sequence alignment of residues in the exo site. (E) Molecular surface of human m-NAD-ME in the active site region, showing the binding modes of ATP and NAD^+.

which are insensitive to fumarate. Therefore, there are additional structural determinants for fumarate binding to human and *A. suum* m-NAD-ME.

The open form I structure of human m-NAD-ME is not compatible with fumarate binding, as the side chain of Phe68 assumes a different conformation and blocks this binding site (*21*). Fumarate may activate the enzyme by promoting the transition from open form I to open form II, which may be more catalytically competent as it requires fewer structural changes to go to closed form II. The presence of fumarate removes the cooperative behavior of the enzyme with respect to the substrate malate (*33*−*35*). The cooperativity is likely due to a coupled transition from open form II to open form I upon malate binding. The presence of fumarate can convert the enzyme monomers to the open form II state, thereby removing the cooperative behavior. This also suggests that the cooperativity occurs within the dimers of the enzyme and is consistent with the Hill coefficient of about 1.5 for the tetramer (*12*).

Exo Site for ATP/NAD^+ Binding. Human m-NAD-ME has an exo site for the binding of ADP, ATP, and the ADP portion of the NAD^+ cofactor (*12*, *21*). This exo site is about 35 Å from the active site (Figure 1A) and is located near the N-terminal end of the parallel β-sheet in domain B and the residues from domain D (Figure 6C). The N6 amino group and the N1 ring nitrogen of the adenine base are specifically recognized in this site. The phosphate groups interact with the side chains of Arg197, Arg542, and Arg556, which are conserved only in human m-NAD-ME (Figure 6D). This exo site may be unique to human m-NAD-ME.

ATP is an inhibitor of human m-NAD-ME (*34*). The structures of human m-NAD-ME in complex with ATP reveal that ATP can bind to the active site as well as the exo site (Figure 6C,E) (*21*). Mutation of the three Arg residues in this site can abolish the binding of ATP to the exo site, but ATP has the same inhibitory potency against these mutants. Kinetic studies show that the inhibition by ATP is competitive with respect to the cofactor NAD^+ or malate (*38*). Therefore, ATP is an active site inhibitor of human m-NAD-ME with a K_i of about 0.2 mM (*21*, *38*). The inhibition of m-NAD-ME by ATP is consistent with its putative role in energy metabolism (*12*). The biological function of the exo site is currently unclear. It may be related to the quaternary structural integrity of m-NAD-ME because mutation at this site will result in dimeric mutants (*38*).

Future Prospects. ME has a tremendous amount of kinetic data available (*4*, *51*, *60*). The rapid progress in structural studies has provided a clear picture of this enzyme never seen before. Combining the kinetic analyses with the structural results allows us to deduce plausible catalytic and allosteric regulation mechanisms of the enzyme. Most of the biochemical analyses results now have a structural basis for interpretation. However, the structure of m-NADP-ME is still unknown. The ME structures from plants and bacteria are also unknown. Furthermore, the structural basis for the half-of-the-site reactivity of the tetrameric c-NADP-ME has not

yet been demonstrated. The structural interconversions proposed in Figure 2 need further experimental verification. Experimental evidence for a distinct structure of the ME−NAD(P)−Mn or the ME−NAD(P)−fumarate ternary complex, the inherent open form II, and the hypothetical closed form II are yet to be established.

Besides the structural work, a valuable tool toward this perspective will be the availability of different dimers with intact tetrameric or dimeric interfaces, respectively. While the tetramer is half-sited, one of the dimers is expected to be half-of-the-sites, but the other should be all-of-the-sites. The monomer, of course, should be all-of-the-sites. In this way, the signal transduction between/among subunits may be elucidated. Intensive site-specific mutagenesis work is now underway to delineate the regulation mode of c-NADP-ME and m-NAD-ME.

ACKNOWLEDGMENT

We thank Paul F. Cook for sharing a manuscript before publication. We also thank our current and former colleagues involved in the work described in this article.

SUPPORTING INFORMATION AVAILABLE

There are 13 crystal structures of malic enzyme in the Protein Data Bank. Table 1 compiles these structures from various sources in different forms. Table 2 lists all contacting amino acid residues that are within 3.5 Å in the A/B, A/C, and A/D subunit pairs in pigeon c-NADP-ME and human m-NAD-ME. This material is available free of charge via the Internet at http://pubs.acs.org.

REFERENCES

1. Kornberg, A. (2001) *J. Biol. Chem. 276*, 3−11.
2. Ochoa, S., Mehler, A. H., and Kornberg, A. (1947) *J. Biol. Chem. 167*, 871−872.
3. Frenkel, R. (1975) *Curr. Top. Cell. Regul. 9*, 157−181.
4. Hsu, R. Y. (1982) *Mol. Cell. Biochem. 43*, 3−26.
5. Goodridge, A. G., Klautky, S. A., Fantozzi, D. A., Baillie, R. A., Hodnett, D. W., Chen, W., Thurmond, D. C., Xu, G., and Roncero, C. (1996) *Prog. Nucleic Acid Res. Mol. Biol. 52*, 89−122.
6. Hill, S., Winning, B., Jenner, H., Knorpp, C., and Leaver, C. (1996) *Biochem. Soc. Trans. 24*, 743−746.
7. Drincovich, M. F., Casati, P., and Andreo, C. S. (2001) *FEBS Lett. 490*, 1−6.
8. Moreadith, R. W., and Lehninger, A. L. (1984) *J. Biol. Chem. 259*, 6215−6221.
9. Reitzer, L. J., Wice, B. M., and Kennell, D. (1979) *J. Biol. Chem. 254*, 2669−2676.
10. Teller, J. K., Fahien, L. A., and Davis, J. W. (1992) *J. Biol. Chem. 267*, 10423−10432.
11. Hassel, B. (2001) *J. Neurosci. Res. 66*, 755−762.
12. Xu, Y., Bhargava, G., Wu, H., Loeber, G., and Tong, L. (1999) *Structure 7*, 877−889.
13. Hsu, R. Y., and Lardy, H. A. (1967) *J. Biol. Chem. 242*, 520−526.
14. Baker, P. J., Thomas, D. H., Barton, C. H., Rice, D. W., and Bailey, E. (1987) *J. Mol. Biol. 193*, 233−235.
15. Clancy, L. L., Rao, G. S. J., Finzel, B. C., Muchmore, S. W., Holland, D. R., Watenpaugh, K. D., Krishnamurthy, H. M., Sweet, R. M., Cook, P. F., Harris, B. G., and Einspahr, H. M. (1992) *J. Mol. Biol. 226*, 565−569.
16. Bhargava, G., Mui, S., Pav, S., Wu, H., Loeber, G., and Tong, L. (1999) *J. Struct. Biol. 127*, 72−75.
17. Tsai, L. C., Kuo, C. C., Chou, W. Y., Chang, G. G., and Yuan, H. S. (1999) *Acta Crystallogr. D55*, 1930−1932.
18. Yang, Z., and Tong, L. (2000) *Protein Pept. Lett. 7*, 287−296.
19. Yang, Z., Batra, R., Floyd, D. L., Hung, H. C., Chang, G. G., and Tong, L. (2000) *Biochem. Biophys. Res. Commun. 274*, 440−444.
20. Yang, Z., Floyd, D. L., Loeber, G., and Tong, L. (2000) *Nat. Struct. Biol. 7*, 251−257.
21. Yang, Z., Lanks, C. W., and Tong, L. (2002) *Structure 10*, 951−960.
22. Tao, X., Yang, Z., and Tong, L. (2003) *Structure 11*, 1141−1150.
23. Yang, Z., Zhang, H., Hung, H. C., Kuo, C. C., Tsai, L. C., Yuan, H. S., Chou, W. Y., Chang, G. G., and Tong, L. (2002) *Protein Sci. 11*, 332−341.
24. Coleman, D. E., Rao, G. S., Goldsmith, E. J., Cook, P. F., and Harris, B. G. (2002) *Biochemistry 41*, 6928−6938.
25. Rao, G. S. J., Coleman, D. E., Karsten, W. E., Cook, P. F., and Harris, B. G. (2003) *J. Biol. Chem. 278*, 38051−38058.
26. Hung, H. C., Chang, G. G., Yang, Z., and Tong, L. (2000) *Biochemistry 39*, 14095−14102.
27. Kuo, C. W., Hung, H. C., Tong, L., and Chang G. G. (2003) *Proteins*, in press.
28. Nevaldine, B. H., Bassel, A. R., and Hsu, R. Y. (1974) *Biochim. Biophys. Acta 336*, 283−293.
29. Chang, G. G., Huang, T. M., and Chang, T. C. (1988) *Biochem. J. 254*, 123−130.
30. Chou, W. Y., Huang, S. M., and Chang, G. G. (1997) *Protein Eng. 10*, 1205−1211.
31. Chou, W. Y., Liu, M. Y., Huang, S. M., and Chang, G. G. (1996) *Biochemistry 35*, 9873−9879.
32. Chang, H. C., Chou, W. Y., and Chang, G. G. (2002) *J. Biol. Chem. 277*, 4663−4671.
33. Landsperger, W. J., and Harris, B. G. (1976) *J. Biol. Chem. 251*, 3599−3602.
34. Sauer, L. A. (1973) *Biochem. Biophys. Res. Commun. 50*, 524−531.
35. Lai, C. J., Harris, B. G., and Cook, P. F. (1992) *Arch. Biochem. Biophys. 299*, 214−219.
36. Chang, G. G., and Hsu, R. Y. (1977) *Biochemistry 16*, 311−320.
37. Hsu, R. Y., and Pry, T. A. (1980) *Biochemistry 19*, 962−968.
38. Hsu, W. C. (2002) M.S. Thesis, National Defense Medical Center, Taipei, Taiwan.
39. Mitsch, M. J., Voegele, R. T., Cowie, A., Osteras, M., and Finan, T. M. (1998) *J. Biol. Chem. 273*, 9330−9336.
40. Hsu, R. Y., Mildvan, A. S., Chang, G. G., and Fung, C. (1976) *J. Biol. Chem. 251*, 6574−6583.
41. Chen, Y. I., Chen, Y. H., Chou, W. Y., and Chang, G. G. (2003) *Biochem. J. 374*, 633−637.
42. Chang, H. C., and Chang, G. G. (2003) *J. Biol. Chem. 278*, 23996−24002.
43. Wei, C. H., Chou, W. Y., Huang, S. M., Lin, C. C., and Chang, G. G. (1994) *Biochemistry 33*, 7931−7936.
44. Wei, C. H., Chou, W. Y., and Chang, G. G. (1995) *Biochemistry* 34, 7949−7954.
45. Karsten, W. E., Chooback, L., Liu, D., Hwang, C.-C., Lynch, C., and Cook, P. F. (1999) *Biochemistry 38*, 10527−10532.
46. Chang, G. G., and Huang, T. H. (1981) *Biochim. Biophys. Acta 660*, 341−347.
47. Rao, S. R., Kamath, B. G., and Bhagwat, A. S. (1991) *Phytochemistry 30*, 431−435.
48. Chang, G. G., and Huang, T. M. (1980) *Biochim. Biophys. Acta 611*, 217−226.
49. Chang, G. G., Shiao, M. S., Liaw, J. G., and Lee, H. J. (1989) *J. Biol. Chem. 264*, 280−287.
50. Satterlee, J., and Hsu, R. Y. (1991) *Biochim. Biophys. Acta 1079*, 247−252.
51. Cleland, W. W. (1999) *Acc. Chem. Res. 32*, 862−868.
52. Liu, D., Karsten, W. E., and Cook, P. F. (2000) *Biochemistry 39*, 11955−11960.
53. Kuo, C. C., Tsai, L. C., Chin, T. Y., Chang, G. G., and Chou, W. Y. (2000) *Biochem. Biophys. Res. Commun. 270*, 821−825.
54. You, K. S. (1985) *CRC Crit. Rev. Biochem. 17*, 313−451.
55. Karsten, W. E., Tipton, P. A., and Cook, P. F. (2002) *Biochemistry 41*, 12193−12199.
56. Viljoen, M., Subden, R. E., Krizus, A., and van Vuuren, H. J. J. (1994) *Yeast 10*, 613−624.
57. Loeber, G., Infante, A. A., Maurer-Fogy, I., Krystek, E., and Dworkin, M. B. (1991) *J. Biol. Chem. 266*, 3016−3021.
58. Wierenga, R. K., Terpstra, P., and Hol, W. G. J. (1986) *J. Mol. Biol. 187*, 101−107.
59. Scrutton, N. S., Berry, A., and Perham, R. N. (1990) *Nature 343*, 38−43.

60. Karsten, W. E., Pais, J. E., Rao, G. S., Harris, B. G., and Cook, P. F. (2003) *Biochemistry 42*, 9712−9721.
61. Glaser, F., Pupko, T., Paz, I., Bell, R. E., Bechor-Shental, D., Martz, E., and Ben-Tal, N. (2003) *Bioinformatics 19*, 163−164.
62. Martz, E. (2002) *Trends Biochem. Sci. 27*, 107−109.
63. Schneider, T. D., and Stephens, R. M. (1990) *Nucleic Acids Res. 16*, 6097−6100.

BI035251+